Self-Assembly of Colloidal Zeolite Precursors into Extended Hierarchically Ordered Solids

C. Shane Carr,[†] Stefan Kaskel,[‡,§] and Daniel F. Shantz*[,†]

Max-Planck-Institut for Coal Research, Muelheim, Germany, and Department of Chemical Engineering, Texas A&M University, College Station, Texas 77843

Received December 7, 2003. Revised Manuscript Received April 14, 2004

A new porous material containing both micropores and mesopores has been synthesized by the self-assembly of silicalite-1 colloidal precursors at low temperatures and thoroughly investigated by diffraction, electron microscopy, porosimetry, and spectroscopy. Our "bottom-up" approach yields mesoporous materials that contain a microporosity different from that of SBA-15. For the samples where the silicalite-1 mixture is aged at room temperature, we do not have conclusive evidence that silicalite-1 is responsible for the microporosity in our samples, as *all* analytical techniques are inconclusive. By contrast, samples where the silicalite-1 mixture is heated until Bragg reflections are observed appear by TEM to be heterogeneous materials containing both mesopores and domains of silicalite-1. Nitrogen and argon adsorption show that both the micropore size distribution and the total micropore volume of our samples are different from those of SBA-15. The conclusions from this study are fourfold: (1) we have created a material containing both micropores and mesopores that is very well ordered on the mesoscale, (2) our material has a larger micropore volume and different micropore size distribution than SBA-15 made under the same conditions, (3) we have achieved this high degree of structural ordering and uniformity without the need for high-temperature syntheses, and (4) it does not appear possible to use larger (∼50 nm) nanoparticles of silicalite-1 to fabricate homogeneous materials. The ability to synthesize these materials at low temperatures makes them (and the synthetic concept) ideal for extension into areas such as thin-film syntheses.

Introduction

Zeolites are a technologically important class of microporous oxides that have found widespread use in catalysis, separations, and ion-exchange operations.[1,2] This is due to their highly crystalline structures, the uniformity of their pores, and the resulting shape selectivity. However, zeolites have some limitations in that their pore sizes are small (<2 nm), inhibiting their ability to process larger molecules. The development of mesoporous silicas and other oxides (MCM-41,[3,4] SBA-15[5−7]) was met with great excitement in the hope that these materials would exhibit the strong acidity of zeolites, allowing one to perform catalytic transformations on large substrates. However, these materials did not exhibit the desired catalytic activity, for the most part because of their low hydrothermal stability and weak acidity.[8] As such, it would be of great interest if one could fabricate mesoporous materials that exhibit the acidity and stability of zeolitic materials.

The synthesis of materials containing both microporosity and mesoporosity is an area that has garnered much interest recently. Starting with the work of Kloetstra et al.,[9] several groups have looked at the synthesis of materials containing a bimodal MCM-41/MFI structure. Many of these have employed a "top-down" approach, taking a mesoporous material and converting its amorphous pore walls into a zeolitic-type material. For instance, Huang et al.[10] examined a two-step crystallization process that involved the transformation of the amorphous wall of MCM-41 directed by the presence of tetrapropylammonium ions. Karlsson et al.[11] reported aggregates of an MCM-41/MFI material synthesized through the embedment of MFI crystals into the MCM-41 material. Poladi et al.[12] examined a two-step process

* Corresponding author: Daniel F. Shantz, Department of Chemical Engineering, Texas A&M University, Mail Stop 3122, College Station, TX 77843-3122. Phone: (979) 845-3492. Fax: (979) 845-6446. E-mail: shantz@che.tamu.edu.

† Texas A&M University.

‡ Max-Planck-Institut for Coal Research.

§ Current address: Institute for Inorganic Chemistry, Technical University Dresden, Helmholtzstrasse 10, Dresden, Germany 01069.

(1) Barrer, R. M. *Hydrothermal Chemistry of Zeolites*; Academic Press: London, 1982.

(2) Breck, D. W. *Zeolite Molecular Sieves*; Wiley: New York, 1974.

(3) Kresge, C. T.; Leonowicz, M. E.; Roth, W. J.; Vartuli, J. C.; Beck, J. S. *Nature* **1992**, *359*, 710.

(4) Beck, J. S.; Vartuli, J. C.; Roth, W. H.; Leonowicz, M. E.; Kresge, C. T.; Schmitt, K. D.; Chu, C. T.; Olson, D. H.; Sheppard, E. W.; McCullem, S. B.; Higgins, J. B.; Schenker, J. L. *J. Am. Chem. Soc.* **1992**, *114*, 10834.

(5) Zhao, D.; Huo, Q.; Feng, J.; Chmelka, B. F.; Stucky, G. D. *J. Am. Chem. Soc.* **1998**, *120*, 6024.

(6) Zhao, D.; Feng, J.; Huo, Q.; Melosh, N.; Fredrickson, G. H.; Chmelka, B. F.; Stucky, G. D. *Science* **1998**, *279*, 548.

(7) Yang, P.; Zhao, D.; Margolese, D. I.; Chmelka, B. F.; Stucky, G. D. *Nature* **1998**, *396*, 152.

(8) Corma, A. *Chem. Rev.* **1997**, *97*, 2373.

(9) Kloetstra, K. R.; van Bekkum, H.; Jansen, J. C. *Chem. Commun.* **1997**, 23, 2281.

(10) Huang, L.; Guo, W.; Deng, P.; Xue, Z.; Li, Q. *J. Phys. Chem. B* **2000**, *104*, 2817.

(11) Karlsson, A.; Stocker, M.; Schmidt, R. *Microporous Mesoporous Mater.* **1999**, *27*, 181.

(12) Poladi, R. H. P. R.; Landry, C. C. *J. Solid State Chem.* **2002**, *167*, 363.

10.1021/cm035283j CCC: $27.50
Published on Web 07/10/2004

that manipulated the growth of the MCM-41 material by introducing the tetrapropylammonium ion during the growth phase of the mesomaterial. Naik et al.[13] studied a dual templating approach that involved the formation of the MFI precursor followed by the addition of a surfactant solution to induce formation of a mesoporous material. Y. Liu et al. examined the utilization of different zeolite seeds reacted with various mesoporous templates including cetyltrimethylammonium bromide, CTAB (MCM-41 template),[14,15] and Pluronic P123 (SBA-15 template)[16] at high temperatures. J. Liu[17] used a TS-1 zeolite precursor with a Pluronic P123 surfactant template at high temperature to form these materials. Xiao and colleagues[18−21] reported the use of clear zeolitic solutions reacted with mesoporous templates at high temperatures to form various ordered mesoporous aluminosilicates, titanosilicates, and a pure silica material, MPS-9,[21] that is used for comparison in this paper. Zhang et al.[22,23] reported the synthesis of a mesoporous aluminosilicate with zeolite-like properties using a dual templating approach. On et al.[24,25] examined syntheses of bimodal materials by the formation of the amorphous mesoporous precursor followed by the crystallization of the amorphous walls with zeolitic precursor. Kremer et al.[26] recently performed an HRTEM study on a dual templating approach in which colloidal silicalite-1 was reacted with either CTAB or Pluronic P123 at relatively high temperatures. It is also of note that there have been numerous investigations of the synthesis and characterization of bimodal micro-/macroscopic materials, starting with the work of Holland et al.[27]

Characterizing these materials poses two primary challenges. The first is that, if one is truly successful in making such micro-/mesoporous materials, the zeolite domains might be sufficiently small to preclude their observation by X-ray diffraction. In this case, demonstrating the existence of the zeolite phase can be achieved, at best, only by using indirect means such as catalytic testing, porosimetry, or spectroscopy. The second case, observation of the zeolite diffraction peaks, demonstrates the presence of the zeolite phase but necessitates exhaustive material investigation by TEM to rule out the possibility that the material is a physical mixture of bulk zeolite and mesoporous solid. In the current work, we observe both cases. Considering the former situation, an IR band at approximately 570 cm^{-1} has been used as a positive indicator that MFI is present;[28] however, many high-silica zeolites (e.g., ZSM-12) exhibit similar bands in the IR region, and studies of as-made SBA-15 performed in our laboratories also show this band at 570 cm^{-1} (vide infra). In both cases, porosimetry can also be employed, but as we discuss below, given the high external surface area/volume ratios of small zeolite particles, this also has complications. Further complications occur because it has been shown that SBA-15 also contains micropores.[29,30] Differentiating between the micropores formed by the polyalkylene oxide block copolymer and any micropores created by a zeolitic phase poses an interesting challenge that must be examined on a more intensive level than routine adsorption analyses such as BET.

We have also decided to examine the synthesis of a micro-/mesoporous MFI/SBA-15 material using a dual templating approach. Our approach has two facets that make it attractive. The first is that we have chosen the "bottom-up" approach for assembling these materials. The second is that we are forming the materials at low temperatures (below 323 K). We have chosen this approach for two reasons. First, it appears to be more amenable to implementation at low temperatures, conditions under which self-assembly is easy to utilize and understand. A major challenge in synthesizing such bimodal materials is preventing the formation of large domains of zeolite (i.e., physically inhomogeneous materials). Also, the ability to form such materials at low temperatures will allow us to extend this synthetic approach beyond powders, for instance, to synthesize hierarchically ordered thin films. This approach is comparable to the synthesis of the MPS-9 materials, but our synthesis does not involve a high-temperature hydrothermal treatment after the initial reaction.

As outlined below we have performed a battery of characterization methods to probe the physicochemical nature of our materials in detail and compared them to MPS-9 and SBA-15 made under the same conditions. We have also studied how preheating the colloidal silicalite-1 mixture impacts the material formed as the silicalite-1 precursor or particle size varies.

Experimental Section

Material Synthesis. The synthesis of the colloidal silicalite-1 mixture was performed as reported earlier (1 TEOS: 0.36 TPAOH:18 H_2O).[31] Nine grams of tetraethoxysilane (>99%, Aldrich) was added to 7.9 g of tetrapropylammonium hydroxide (40 wt %, Alfa Aesar), and the mixture was stirred at room temperature for 30 min. Deionized water (9 mL) was added, and the mixture was stirred at room temperature for 60 min. After this time, the mixture appears to be a single phase. In a separate vessel, 4.2 g of Pluronic P123 was dissolved in 4 M HCl and water at room temperature. Two Pluronic mixtures (low acid, high acid) were used. The low-

(13) Naik, S. P.; Chiang, A. S. T.; Thompson, R. W.; Huang, F. C.; Kao, H.-M. *Microporous Mesoporous Mater.* **2003**, *60*, 213.
(14) Liu, Y.; Zhang, W.; Pinnavaia, T. J. *Angew. Chem., Int. Ed.* **2001**, *40*, 1255.
(15) Liu, Y.; Zhang, W.; Pinnavaia, T. J. *J. Am. Chem. Soc.* **2000**, *122*, 8791.
(16) Liu, Y.; Pinnavaia, T. J. *Chem. Mater.* **2002**, *14*, 3.
(17) Liu, J.; Zhang, X.; Han, Y.; Xiao, F.-S. *Chem. Mater.* **2002**, *14*, 2536.
(18) Han, Y.; Wu, S.; Sun, Y.; Li, D.; Xiao, F.-S.; Liu, J.; Zhang, X. *Chem. Mater.* **2002**, *14*, 1144.
(19) Han, Y.; Xiao, F.-S.; Wu, S.; Sun, Y.; Meng, X.; Li, D.; Lin, S.; Deng, F.; Ai, X. *J. Phys. Chem. B* **2001**, *105*, 7963.
(20) Xiao, F.-S.; Han, Y.; Yu, Y.; Meng, X.; Yang, M.; Wu, S. *J. Am. Chem. Soc.* **2002**, *124*, 888.
(21) Han, Y.; Li, N.; Zhao, L.; Li, D.; Xu, X.; Wu, S.; Di, Y.; Li, C.; Zou, Y.; Yu, Y.; Xiao, F.-S. *J. Phys. Chem. B* **2003**, *107*, 7551.
(22) Zhang, Z.; Han, Y.; Xiao, F.-S.; Qiu, S.; Zhu, L.; Wang, R.; Yu, Y.; Zhang, Z.; Zou, B.; Wang, Y.; Sun, H.; Zhao, D.; Wei, Y. *J. Am. Chem. Soc.* **2001**, *123*, 5014.
(23) Zhang, Z.; Han, Y.; Zhu, L.; Wang, R.; Yu, Y.; Qiu, S.; Zhao, D.; Xiao, F.-S. *Angew. Chem., Int. Ed.* **2001**, *40*, 1258.
(24) On, D. T.; Kaliaguine, S. *Angew. Chem., Int. Ed.* **2001**, *40*, 3248.
(25) On, D. T.; Kaliaguine, S. *Angew. Chem., Int. Ed.* **2002**, *41*, 1036.
(26) Kremer, S. P. B.; Kirschhock, C. E. A.; Aerts, A.; Villani, K.; Martens, J. A.; Lebedev, O. I.; Tendeloo, G. V. *Adv. Mater.* **2003**, *15*, 1705.
(27) Holland, B. T.; Abrams, L.; Stein, A. *J. Am. Chem. Soc.* **1999**, *121*, 4308.
(28) Ravishankar, R.; Kirschhock, C. E. A.; Verspeurt, F.; Grobet, P. J.; Jacobs, P. A.; Martens, J. A. *J. Phys. Chem. B* **1999**, *103*, 4965.
(29) Imperor-Clerc, M.; Davidson, P.; Davidson, A. *J. Am. Chem. Soc.* **2000**, *122*, 11925.
(30) Ravikovitch, P. I.; Neimark A. V. *J. Phys. Chem. B* **2001**, *105*, 6817.
(31) Schoeman, B. J.; Regev, O. *Zeolites* **1996**, *17*, 447.

acid synthesis (LA) employed 30 mL of 4 M HCl in 105 mL of water, and the high-acid synthesis (HA) employed 60 mL of 4 M HCl in 75 mL of water. The MFI mixture was added to the polymer solution and allowed to react at various temperatures (23−50 °C) for 24 h. The resulting solids were filtered, washed with deionized water, and calcined at 550 °C for 8 h. For clarity hereafter, the materials are identified as MM-acidity-temperature, so MM-LA-35 represents a low-acid synthesis at 35 °C. To assess materials that should contain different silicalite-1 domain sizes, we also prepared samples where the colloidal silicalite-1 mixture was heated for different periods of time at 95 °C (6 and 18 h), cooled to room temperature, and added to the Pluronic mixture and aged for 24 h at 35 °C. These samples are referred to below as MM-LA-35-H6 and MM-LA-35-H18, respectively, where H*x* refers to the fact that the silicalite-1 solutions were heated for *x* hours at 95 °C.

The SBA-15 materials were made by dissolving 4.2 g of Pluronic P123 in 60 mL of 4 M HCl and 85 mL of distilled water. TEOS (8.5 g) was added, and the mixture was stirred at various temperatures (23−50 °C) for 24 h. The resulting solids were filtered, washed with deionized water, and calcined at 550 °C for 8 h. MPS-9 was synthesized using the procedure reported previously.[21]

Characterization. Transmission electron microscopy was performed on a JEOL 2010 microscope with a lanthanum hexaboride filament and an excitation voltage of 200 kV. The samples were ground with a mortar and pestle and then dispersed in ethanol (100%, Aldrich) and placed on a 400-mesh copper grid. Numerous images were taken for each sample at various locations to ensure that the images were representative of the bulk materials.

Powder X-ray diffraction (XRD) was performed on a Bruker-AXS D8 powder diffractometer using Cu Kα radiation. Samples were analyzed over a range of 0.8−30° 2θ using a step scan mode with a step size of 0.01° and a step rate of 5 s/step. Peak intensities and 2θ values were determined using the Bruker program EVA.

Infrared spectroscopy was performed on a Thermo Nicolet Nexus 670 FTIR instrument. Background spectra were collected after 30 min of evacuation. A powder mixture of mass ratio 0.01 sample:0.99 potassium bromide (Aldrich) was pelletized and analyzed after 30 min of evacuation. One hundred twenty-eight scans were acquired per spectrum. ^{29}Si solid-state NMR spectra were measured on a Bruker MSL 300 spectrometer at 59.63 MHz. Chemical shifts are referenced to tetramethylsilane. One-pulse ^{29}Si MAS NMR spectra were acquired using a 7-mm probe with ZrO_2 rotors, a spinning rate of 3 kHz, a 4-μs 60° pulse, high-power proton decoupling, and a 120-s recycle delay to avoid relaxation effects in the signal intensities.

Nitrogen adsorption experiments were performed on a Micromeritics ASAP 2010 micropore analyzer with a turbopump capable of obtaining relative pressures of less than 10^{-6}. About 0.1−0.2 g of sample was degassed under vacuum at 100 °C for 4 h and then at 300 °C for 20 h before analysis was performed. The experiments were conducted in a liquid nitrogen bath at 77 K. The analysis was performed at relative pressures ranging from 10^{-6} to 0.988. Surface area and pore volumes were determined by the α_s method.[32,33] Micropore size distributions were determined from nitrogen and argon porosimetry at 77 K using the Horvath−Kawazoe method using a cylindrical pore geometry.[34−37] The mesopore size distribution was calculated from the adsorption branch of the isotherm using the BJH method with a modified equation for the statistical film thickness.[38,39]

α_s Analysis. The first step required in the α_s analysis was to obtain the isotherm for a reference nonporous material with chemical surface properties similar to those of the experimental sample.[29,30] A nonporous silica material, LiChrospher Si-1000,[40] was used as the reference material for the α_s analysis. This isotherm can be converted to an α_s plot by dividing each respective volume adsorbed by the volume adsorbed at a relative pressure of 0.4. This dimensionless volume is defined as α_s. The measured α_s values were plotted versus their respective relative pressures, and $\alpha_s(p/p_o)$ was obtained through curve fitting. This relationship was then used for all of the experimental work to convert relative pressure to α_s values. This conversion was made for each of the samples, and the adsorbed volume was then plotted versus α_s. Information such as surface areas and pore volumes could be determined by analysis of the α_s plot. Analysis of the α_s plots has been described previously.[32,33]

Results and Discussion

In the current work, we studied how numerous parameters impact the final properties of the material. In the interest of space, some of the findings will be summarized here and not expounded below. In general, we observed that the final material properties were insensitive to the acid content of the synthesis mixture. We also found that aging the colloidal silicalite-1 solution mixture at room temperature for more than 1 h had little effect. We performed aging studies up to 2 weeks in duration with no apparent effect on the material obtained according to XRD, TEM and absorption analyses. We also found that the material properties of the MM materials were not strongly affected by synthesis temperature between the range of 293−343 K. With these points in mind, the results discussed below focus on two points: (i) a comparison of how MM-LA-35 differs from SBA-15 made at 308 K and from MPS-9 and (ii) an investigation of how heating the colloidal silicalite-1 mixture at 368 K for various periods (6, 18 h) before adding it to the Pluronic mixture impacts the final material properties. This second item was studied because we do not observe silicalite-1 by X-ray diffraction in the materials where the silicalite-1 mixture is aged only at room temperature. There are contradictory results in the literature pertaining to the exact nature of the colloidal particles in TEOS/TPAOH/H_2O solutions and when they form crystalline silicalite-1.[28,31,41−43] We do not attempt to resolve this issue here, but rather note that the TEOS/TPAOH/H_2O mixtures we heated in this work before synthesizing our micro-/mesoporous material were heated long enough that crystalline silicalite-1 should be present according to a consensus of the existing literature.[28,31,41,43]

X-ray Diffraction. The low-angle X-ray diffraction patterns for calcined MM-LA-35, SBA-15-35, and MPS-9 are shown in Figure 1 (top). The pattern shows both the SBA-15 and our material to be of hexagonal symmetry with three distinct peaks that can be indexed as the (100), (110), and (200) reflections. The MPS-9

(32) Gregg, S. J.; Sing, K. S. W. *Adsorption, Surface Area, and Porosity*; Academic Press: London, 1982.
(33) Rouquerol, F.; Rouquerol, J.; Sing, K. *Adsorption by Powders and Porous Solids*; Academic Press: London, 1999.
(34) Saito, A.; Foley, H. C. *Microporous Mater.* **1995**, *3*, 531.
(35) Saito, A.; Foley, H. C. *Microporous Mater.* **1995**, *3*, 543.
(36) Saito, A.; Foley, H. C. *AIChE J.* **1991**, *37*, 429.
(37) Horvath, G.; Kawazoe, K. *J. Chem. Eng. Jpn.* **1983**, *16*, 470.
(38) Barrett, E. P.; Joyner, L. G.; Halenda, P. P. *J. Am. Chem. Soc.* **1951**, *73*, 373.
(39) Kruk, M.; Jaroniec, M.; Sayari, A. *Langmuir* **1997**, *13*, 6267.
(40) Jaroniec, M.; Kruk, M.; Olivier, J. P. *Langmuir* **1999**, *15*, 5410.
(41) Kragten, D. D.; Fedeyko, J. M.; Sawant, K. R.; Rimer, J. D.; Vlachos, D. G.; Lobo, R. F.; Tsapatsis, M. *J. Phys. Chem. B* **2003**, *107*, 10006.
(42) Ravishankar, R.; Kirschhock, C. E. A.; Knops-Gerrits, P.-P.; Feijen, E. J. P.; Grobet, P. J.; Vanoppen, P.; De Schryver, F. C.; Miehe, G.; Feuss, H.; Schoeman, B. J.; Jacobs, P. A.; Martens, J. A. *J. Phys. Chem. B* **1999**, *103*, 4960.
(43) Mintova, S.; Olson, N. H.; Senker, J.; Bein, T. *Angew. Chem., Int. Ed.* **2002**, *41*, 2558.

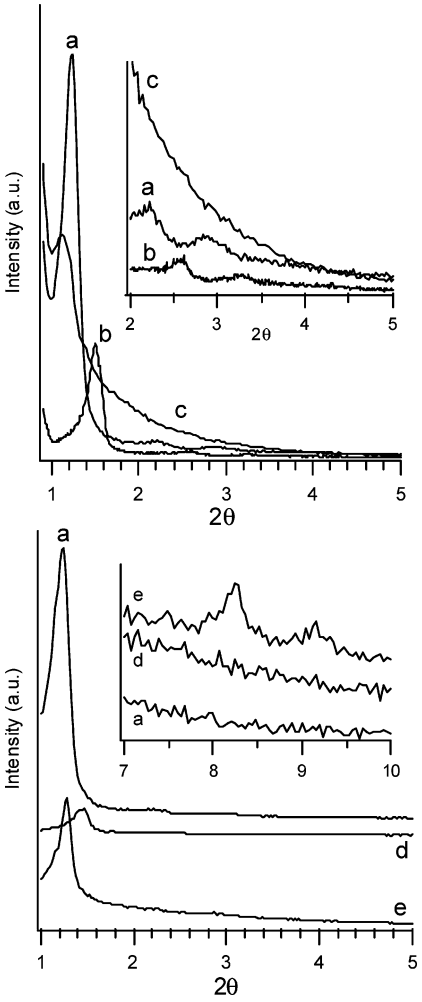

Figure 1. Powder X-ray diffraction patterns of (top) (a) MM-LA-35, (b) SBA-15-35, and (c) MPS-9 and (bottom) (d) MM-LA-35-H6 and (e) MM-LA-35-H18.

sample appears to be much less ordered, which is consistent with the findings of Han et al.[21] The (100) peak of MM-LA-35 is at a *d* spacing of 71.7 Å, corresponding to a unit cell parameter of 8.3 nm. All of the samples made using our experimental procedure exhibit three peaks in the diffraction pattern, consistent with a hexagonal mesostructure. We do not observe diffraction peaks between 7 and 10° 2θ for silicalite-1 in sample MM-LA-35 (Supporting Information). Figure 1 (bottom) shows the low-angle XRD data MM-LA-35, MM-LA-35-H6, and MM-LA-35-H18. Although there are not appreciable differences in the location of the (100) peak, diffraction peaks at 8.3° and 9.2° 2θ can be observed for the MM-LA-35-H18 sample, but not for the MM-LA-H6 sample. The appearance of these peaks supports the presence of crystalline silicalite-1 in this sample. Small-angle X-ray scattering (SAXS) measurements in our laboratory[44] indicate that, after 6 and 18 h at 368 K, the particles in the silicalite-1 mixtures are approximately 6 and 45 nm in diameter, respectively. A key point we will revisit later is the comparison of the particle size by SAXS to the wall thickness of the materials by TEM (see below). The high-angle XRD data

(44) Cheng, C.-H.; Shantz, D. F. Texas A&M University, College Station, TX. Unpublished data.

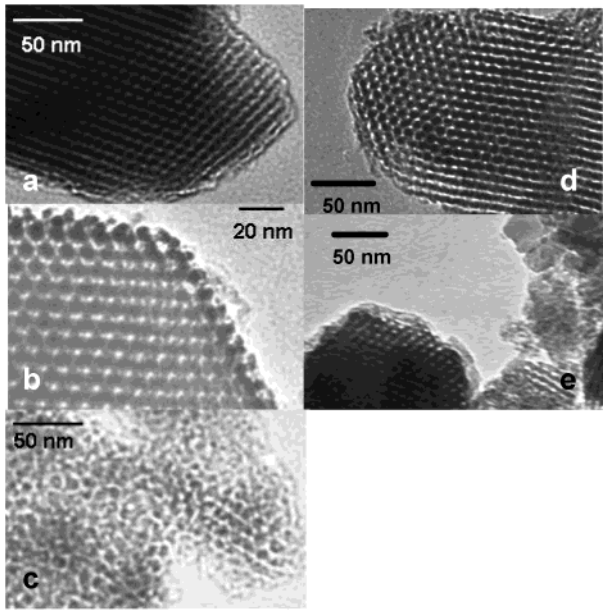

Figure 2. TEM images of (a) MM-LA-35, (b) SBA-15-35, (c) MPS-9, (d) MM-LA-35-H6, and (e) MM-LA-35-H18.

(Supporting Information) for these three samples along with Cabosil (Cabot) show that a broad peak at 22° 2θ of amorphous silica (Cabosil) is essentially absent in the MM-LA-35 sample and has shifted substantially in the two heated samples, consistent with previous work.[43] We also observe a very weak diffraction peak at 23.4° 2θ for the sample heated 18 h, which is likely the (501) reflection of silicalite-1.

The primary mesopore size is calculated using eq 1, where c is a constant equal to 1.213 for circular pores and 1.155 for hexagonal pores; ρ is the pore wall density, which is assumed to be 1.6 g/cm^3 for these materials (2.2 g/cm^3 for amorphous silica); d is the d spacing determined by XRD, and V_p is the mesopore volume.[39]

$$w_d = cd\left(\frac{\rho V_p}{1 + \rho V_p}\right)^{(1/2)} \quad (1)$$

Assuming that the pores are cylindrical, the primary mesopore size for MM-LA-35 is 5.6 nm, which, using the unit cell parameter, yields a wall thickness of 2.7 nm. The SBA-15-35 material has a unit cell parameter of 6.8 nm, a calculated mesopore size of 4.4 nm, and a wall thickness of 2.4 nm. The unit cell parameters, calculated mesopore sizes, and wall thicknesses for (i) MM-LA-35-H6 and (ii) MM-LA-35-H18 are (i) 7.0, 5.2, and 1.8 nm and (ii) 8.0, 5.5, and 2.5 nm, respectively. The wall thickness is lower for the MM-LA-H6 sample as compared to the SAXS results, although the values are comparable. However, the wall thickness for MM-LA-35-H18 is 5% of the size of the silicalite-1 particles observed by SAXS after heating for 18 h. Given that we observe Bragg crystallinity in the final material for MM-LA-35-H18, this result would suggest that this material is a physical mixture of silicalite-1 and mesoporous material.

Transmission Electron Microscopy. Hexagonally ordered mesopores are clearly observed by TEM (Figure 2). Analysis of the MM-LA-35 image shows the pore diameter to be approximately 6 nm and the wall

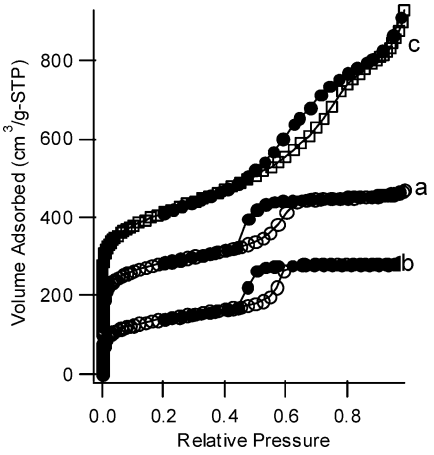

Figure 3. Nitrogen adsorption isotherms for (a) MM-LA-35, (b) SBA-15-35, and (c) MPS-9. Open and closed symbols correspond to the adsorption and desorption branches, respectively. a and c are offset 100 and 200 cm^3/g (STP), respectively.

thickness to be approximately 3 nm. These values, within the error of the measurements, are the same as those calculated from X-ray diffraction. On the basis of repeated analyses of multiple domains in multiple samples, we conclude that these materials are homogeneous by TEM and not physical mixtures of mesoporous silica and other phases. TEM also shows the SBA-15-35 material to contain well-ordered mesopores with a pore diameter of 4.5 nm, in good agreement with the XRD findings. The TEM results for MPS-9 show the materials to be mainly amorphous with localized areas of disordered hexagonal structure. This is consistent with findings in previous work.[21] The TEM and XRD results are in good agreement in that our materials contain a well-ordered mesopore system. MM-LA-35-H6 appears to show a well-ordered mesostructure with a mesopore size of approximately 6 nm. MM-LA-35-H18 also shows areas that contain domains of ordered 6-nm mesopores, but this sample appears to be far less homogeneous than the other samples. This is consistent with the interpretation of the XRD results for this sample, which indicate that it is a physical mixture of mesoporous silica and silicalite-1. It seems unlikely that the domains lacking mesopores are amorphous given that the high-angle XRD data appear very different from the corresponding data for amorphous silica. This is consistent with the results from the XRD and small-angle X-ray scattering analyses. The estimated wall thicknesses for the two heated samples are 1.7 nm for MM-LA-35-H6 and 2.5 nm for MM-LA-35-H18. Both values are in good agreement with the findings from XRD.

Adsorption Analysis. Nitrogen adsorption/desorption isotherms of MM-LA-35, SBA-15, and MPS-9 are shown in Figure 3. The shape of the isotherms is that of a typical type IV isotherm, except in the low-relative-pressure region where the curve exhibits type I properties.[32,33] This indicates the presence of both micro- and mesopores. In the very low relative pressure region ($p/p_o < 0.0001$), the slope of the isotherm is very steep, which is indicative of micropore filling (Figure 4). The sharp adsorption and desorption branches of the hysteresis loop indicate the presence of uniformly sized

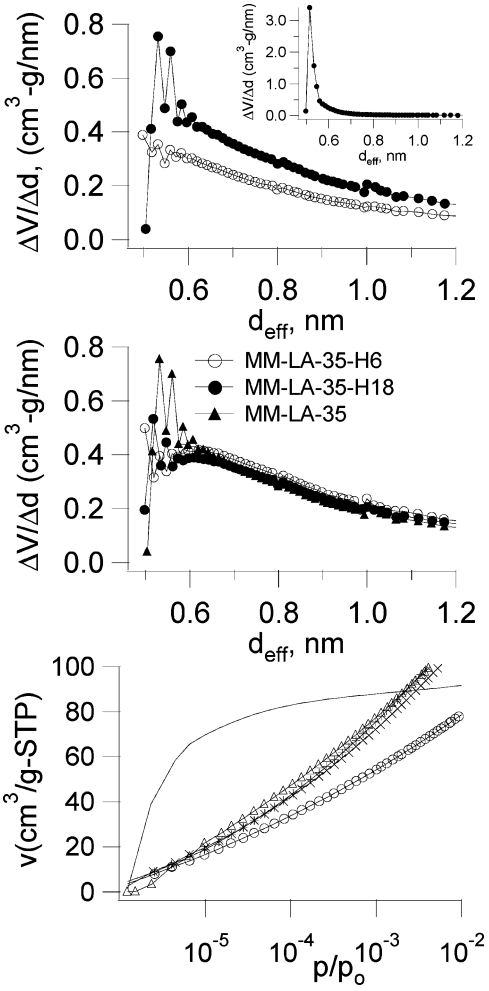

Figure 4. (Top) Micropore size distribution of MM-LA-35 (●) and SBA-15-35 (○). Inset is for silicalite-1. (Middle) Micropore size distributions of MM-LA-35, MM-LA-35-H6 and MM-LA-35-H18. (Bottom) Nitrogen adsorption isotherms of silicalite-1 (solid line), SBA-15-35 (○), MM-LA-35 (△), MM-LA-35-H6 (+), and MM-LA-35-H18 (×).

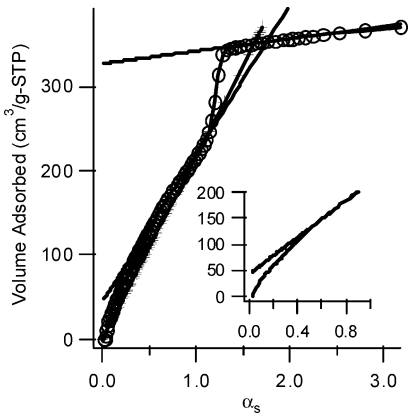

Figure 5. α_s plot of MM-LA-35 nitrogen adsorption data.

mesopores. These hysteresis loops are located in the relative pressure range of 0.4−0.7. Nitrogen adsorption was used for the determination of the mesopore size distribution, the surface area, and the mesopore volume. The total surface areas and pore volumes for (i) MM-LA-35, (ii) SBA-15-35, and (iii) MPS-9 determined by the α_s method are (i) 658 m^2/g and 0.51 cm^3/g, (ii) 505

Table 1. Results from Nitrogen and Argon Adsorption Analysis

characteristic	units	MM-LA-35	SBA-15-35	MM-LA-35-H6	MM-LA-35-H18	MPS-9
BET surface area	m^2/g	658	505	710	667	730
total surface area	m^2/g	594	451	646	623	742
total pore volume	cm^3/g	0.51	0.44	0.53	0.46	0.53
micropore volume	cm^3/g	0.07	0.04	0.05	0.04	~0
mesopore volume	cm^3/g	0.44	0.40	0.48	0.42	~0.53
mesopore size	nm	5.8	5.7	5.9	5.9	9.0

m^2/g and 0.44 cm^3/g, and (iii) 742 m^2/g and 0.53 cm^3/g. (See Figure 5 for the α_s plot for sample MM-LA-35.) On inspection, the surface area for SBA-15-35 is lower than expected; however, this is because the synthesis temperature (35 °C) employed here is lower than what is typically used (80 °C), and it has been shown that increased synthesis temperatures lead to higher pore volumes and surface areas.[5] The nitrogen adsorption isotherms for (iv) MM-LA-35-H6 and (v) MM-LA-35-H18 are comparable to that of the MM-LA-35 sample (Supporting Information). The materials have total surface areas and pore volumes of (iv) 710 m^2/g and 0.53 cm^3/g and (v) 667 m^2/g and 0.46 cm^3/g. The mesopore size distributions (PSDs) were determined using the BJH formalism,[38] assuming cylindrical pores and using the parameters developed by Jaroniec et al.[39] for mesoporous silicas

$$t(p/p_o) = 0.1\left[\frac{60.65}{0.03071 - \log(p/p_o)}\right]^{0.3968} \quad (2)$$

$$r(p/p_o) = \frac{\gamma V_L}{RT \ln(p_o/p)} + t(p/p_o) + 0.3 \quad (3)$$

where γ is the liquid adsorbate surface tension and V_L is the molar volume of the liquid adsorbate (0.00888 N/m and 34.68 cm^3/mol respectively). The Harkins–Jura representation (eq 2) is valid only for the relative-pressure region between 0.1 and 0.95, so a different framework must be used to estimate the micropore size distribution (vide infra). In the mesopore region, the PSDs typically show one strong maximum for pore sizes between 5.5 and 6.3 nm (Supporting Information). As the synthesis temperature was increased, the observed trend was for larger pores to form, as was evidenced by the PSD data. This trend is also observed in the synthesis of SBA-15[5] and is a result of the decreased solubility of the PEO block with increasing temperature.[45] For MM-LA-35, the primary mesopore size was determined to be 5.8 nm as compared to a mesopore size of 5.7 nm for SBA-15-35; these are the same within the error of the method. The MM-LA-35 values agree well with the XRD and TEM results, but the SBA-15-35 values do not for unknown reasons. MPS-9 showed a broad range of mesopores between approximately 9–11 nm. Both MM-LA-35-H6 and MM-LA-35-H18 exhibit a mesopore size of 5.9 nm. That all samples made at 35 °C have the same mesopore size is consistent with previous work that shows that the synthesis temperature strongly determines the mesopore size through the temperature-dependent solubility of the PEO and PPO blocks.[5]

Nitrogen and argon adsorption were used to determine the micropore size distributions and micropore volumes of the samples (Table 1). The cylindrical pore model (eq 4) derived by Everett and Powel's cylindrical potential model[46] was used

$$\ln(p/p_o) = \epsilon_o^* \sum_{k=0}^{\infty} \left\{ \frac{1}{k+1} \left(1 - \frac{d_o}{r}\right)^{2k} \left[\frac{21}{32} \alpha_k \left(\frac{d_o}{r}\right)^{10} - \beta_k \left(\frac{d_o}{r}\right)^4 \right] \right\} \quad (4)$$

The constants necessary for the implementation of the model were found in reported works by Saito and Foley[34–36] and Horvath and Kawazoe.[37] The differential volume divided by the differential effective diameter for each pressure step was calculated and plotted versus the effective pore diameter. The micropore size distributions from nitrogen adsorption are shown in Figure 4. MM-LA-35 and MM-LA-35-H18 each show two peaks between 0.5 and 0.6 nm. The silicalite-1 peak is significantly stronger than all of the observed samples and is at approximately 0.55 nm, in good agreement with previous results.[34–36] The SBA-15-35 material shows a broader PSD and lower pore volumes in the pore size range of 0.5–0.7 nm, comparatively similar to the approximated 5-Å micropores found by HRTEM in previous work.[17] MPS-9 does not appear to exhibit appreciable microporosity and therefore is not shown. MM-LA-35-H18 and MM-LA-H6 shows micropore size maxima closer to 0.6 nm and have slightly lower micropore volumes than MM-LA-35 but higher micropore volumes than SBA-15-35.

Because of the presence of micropores in the native SBA-15 material, it is impossible to comment conclusively on the micropore structure relying exclusively on porosimetry. However, the different pore size distributions between the materials suggest that the micropores in our materials are not the same as those in SBA-15. Also, there is a substantial difference in the micropore volumes of the two samples: 0.07 cm^3/g for MM-LA-35 and 0.04 cm^3/g for SBA-15-35. This difference, although not large in absolute terms, is large in relative terms (~75% increase in micropore volume) and is completely reproducible between samples. We also measured argon isotherms at 77 K, and those results are consistent with the nitrogen adsorption. One complication for the argon adsorption results is that the experiments were run at 77 K (triple point of nitrogen) rather than at 87 K (triple point of argon). This might have led to the freezing of the argon within the sample tube and, therefore, skewing of the analysis. As a result, we feel that the nitrogen adsorption data are more reliable. The argon adsorption results are consistent with low-pressure nitrogen adsorption results showing the MM-LA-35 and SBA-15-35 to have micropore volumes of 0.09 and 0.06 cm^3/g, respectively. The two heated samples have the following

(45) Zana, R. *Colloids Surf. A* **1999**, *123–124*, 27.

(46) Everett, D. H.; Powl, J. C. *J. Chem. Soc.* **1976**, *72*, 619.

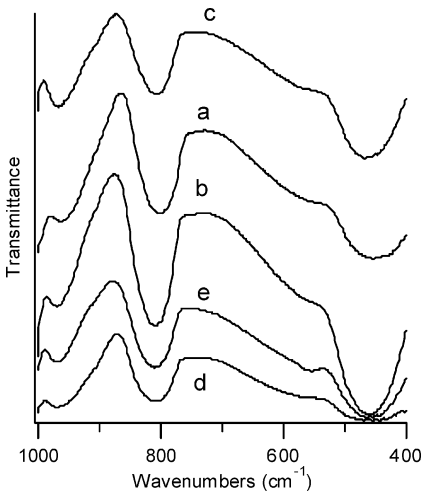

Figure 6. IR spectra of as-made (a) MM-LA-35, (b) SBA-15-35, (c) MPS-9, (d) MM-LA-35-H6, and (e) MM-LA-35-H18.

micropore volumes according to the nitrogen and argon adsorption results, respectively: (i) H6, 0.05 and 0.07 cm^3/g; (ii) H18, 0.04 and 0.07 cm^3/g. Although we believe some caution is in order regarding the pore size values, the important result here is that our materials and the SBA material exhibit differences in the terms of both the micropore volumes and the relative size of the micropores.

Infrared and NMR Spectroscopy. Several reports exist that attribute a strong peak at 570 cm^{-1} to the presence of double five-membered silica rings. This feature in IR spectra has been used[28] as an indicator for the presence of MFI. Both the as-made SBA-15 and as-made MM-materials exhibit this peak (Figure 6), indicating that this peak cannot be reliably used as a means of phase identification. This peak disappears upon calcination, although a slight inflection remains at this point. Further, other work in our laboratory investigating other high-silica zeolites (e.g., ZSM-12) has found this peak in the IR spectra of such materials as well. Also of note is that the band is no more pronounced for the calcined material that displays Bragg reflections for silicalite-1 than for the other samples. Our results as well as others in the literature[41] show that attempting to use IR spectroscopy for phase identification is misleading. Here, we show that several materials containing different microstructures look similar by IR spectroscopy, and as such, FTIR spectroscopy is not a conclusive method for phase assessment as X-ray diffraction is for bulk samples.

The ^{29}Si MAS NMR spectra of SBA-15-35 and MM-LA-35 do not show any appreciable differences. The spectra of MM-LA-35 appear very similar to those reported of solids extracted from silicalite-1 clear-solution syntheses.[41] As observed in previous studies, the spectra are comparable to those of X-ray amorphous materials.

One thing we did not study in detail here was the synthesis of micro-/mesoporous materials containing heteroatoms (e.g., aluminum). There were two reasons we chose not to pursue this issue. First, our interest was in attempting to understand the material synthesis, and all-silica systems facilitate that. Second, catalytic testing, although useful, is again at best an indirect probe of the presence of a zeolite phase and provides no information about whether materials are homogeneous or inhomogeneous. Preliminary work performed on synthesizing aluminum-containing MM-LA-35 samples was unsuccessful. This is not surprising given the high solubility of alumina at low pH.[47] How these materials perform catalytically is certainly of interest, and we are currently exploring this topic.

Conclusions

Our bottom-up approach yields mesoporous materials that contain a microporosity different from that of SBA-15. For the samples where the silicalite-1 mixture is aged at room temperature, we do not have conclusive evidence that silicalite-1 is responsible for the microporosity in our samples, as *all* analytical techniques are inconclusive. By contrast, samples where the silicalite-1 mixture is heated until Bragg reflections are observed appear by TEM to be heterogeneous materials containing both mesopores and domains of silicalite-1. TEM and IR and NMR spectroscopies are all inconclusive in identifying the micropore structure. Nitrogen and argon adsorption show that both the micropore size distribution and the total micropore volume of our samples are different from those of SBA-15. Therefore, the conclusions from this study are fourfold: (1) we have created a material containing both micropores and mesopores that is very well ordered on the mesoscale, (2) our material has a larger micropore volume and different micropore size distribution than SBA-15 made at the same conditions, (3) we have achieved this high degree of structural ordering and uniformity without the need for high-temperature syntheses, and (4) it does not appear possible to use larger (∼50 nm) nanoparticles of silicalite-1 to fabricate homogeneous materials. The ability to synthesize these materials at low temperatures makes them (and the synthetic concept) ideal for extension into areas such as thin-film syntheses. Our work also shows the challenges the materials chemistry community faces in quantifying the microstructure of these micro-/mesoporous materials.

Acknowledgment. This work was supported by the Texas Advanced Research Program. C.S.C. gratefully acknowledges the Center for Integrated Microchemical Systems at Texas A&M for support. D.F.S. and C.S.C. acknowledge an NSF International Travel Award to support collaborative work at the Max-Planck-Institute for Coal Research in Mulheim Germany (INT-0234302). S.K. acknowledges support from the DAAD for travel to Texas A&M University. The authors acknowledge B. Ziborwius at MPI-Muelheim for selected ^{29}Si NMR measurements and useful discussions. The authors gratefully acknowledge C. Dybowski and S. Bai at the Department of Chemistry and Biochemistry at the University of Delaware for use of the NMR facilities and BASF for the donation of the Pluronic surfactant. The authors also thank the reviewers for useful comments.

Supporting Information Available: Low-relative-pressure data for nitrogen adsorption isotherms (Table S1); powder

(47) Brinker, C. J.; Scherer, G. W. *Sol−Gel Science: The Physics and Chemistry of Sol−Gel Processing*; Academic Press: Boston, 1990.

XRD patterns of MM-LA-35, SBA-15-35, and MPS-9 (Figure S1); high-angle XRD data for MM-LA-35, MM-LA-35-H6, MM-LA-35-H18, and Cabosil (Figure S2); nitrogen adsorption isotherms for MM-LA-35-H6 and MM-LA-35-H18 (Figure S3); mesopore size distributions for MM-LA-35, SBA-15-35, MM-LA-35-H6, MM-LA-35-H18, and MPS-9 (Figure S4). This material is available free of charge via the Internet at http://pubs.acs.org.

CM035283J